

Observational indications of magneto-optical effects in the scattering polarization wings of the Ca I 4227 Å line

Emilia Capozzi,¹ Ernest Alsina Ballester,¹ Luca Belluzzi,^{1,2} Michele Bianda,¹ Sajal Kumar Dhara,¹ and Renzo Ramelli¹

¹ Istituto Ricerche Solari Locarno, 6605 Locarno Monti, Switzerland
e-mail: emilia.capozzi@irsol.ch

² Leibniz-Institut für Sonnenphysik (KIS), 79104 Freiburg, Germany

Preprint online version: July 24, 2020

ABSTRACT

Context. Several strong resonance lines, such as H I Ly- α , Mg II k, Ca II K, Ca I 4227 Å, which are characterized by deep and broad absorption profiles in the solar intensity spectrum, show conspicuous linear scattering polarization signals when observed in quiet regions close to the solar limb. Such signals show a characteristic triplet-peak structure, with a sharp peak in the line core and extended wing lobes. The line core peak is sensitive to the presence of magnetic fields through the Hanle effect, which however is known not to operate in the line wings. Recent theoretical studies indicate that, contrary to what was previously believed, the wing linear polarization signals are also sensitive to the magnetic field through magneto-optical effects.

Aims. We search for observational indications of this recently discovered physical mechanism in the scattering polarization wings of the Ca I 4227 Å line.

Methods. We performed a series of spectropolarimetric observations of this line using the Zurich IMaging POLarimeter (ZIMPOL) camera at the Gregory-Coudé telescope of IRSOL (Switzerland) and at the GREGOR telescope in Tenerife (Spain).

Results. Spatial variations of the total linear polarization degree and of the linear polarization angle are clearly appreciable in the wings of the observed line. We provide a detailed discussion of our observational results, showing that the detected variations always take place in regions where longitudinal magnetic fields are present, thus supporting the theoretical prediction that they are produced by MO effects.

Key words. Polarization, scattering, Sun: photosphere, chromosphere, magnetic fields, Techniques: polarimetric

1. Introduction

Over a decade ago, unexpected observations of the scattering polarization signal of the Ca I 4227 Å line were reported (see Bianda et al. 2003). This signal shows a triplet-peak structure, with a sharp peak in the line core, and broad lobes in the wings. The wing lobes, which are typical of strong resonance lines, are produced by coherent scattering processes. The observations of Bianda et al. (2003) were unexpected because, in addition to spatial variations in the Stokes Q/I wing signal (the reference direction for positive Q being the parallel to the closest limb), U/I wing signals of substantial amplitude and showing similar spatial variations were found. While spatial variations of the Q/I wing lobes could in principle be explained in terms of variations of the anisotropy of the radiation field, or of particular properties of the atmospheric plasma (e.g., the density of neutral perturbers, which determine the fraction of coherent scattering processes), no straightforward physical explanation was readily available for the appearance and variation of U/I wing signals.

The observation of U/I signals in the line wings could not be explained in terms of the Hanle effect, as this is known to operate in the core of spectral lines and not in the wings (for an exhaustive overview, see Stenflo 1982; Trujillo Bueno 2001; Landi Degl’Innocenti & Landolfi 2004). This circumstance actually lead to the common belief that the large wing scattering polarization signals shown by strong resonance lines were insensitive to the presence of magnetic fields. On the other hand, Bianda et al. (2003) reported that the observed variations in the Q/I and

U/I wings of the Ca I 4227 Å line were always accompanied by Zeeman signals in the nearby blends, thus suggesting that such unexpected wing behavior could indeed have a not yet understood magnetic origin. Sampoorana et al. (2009) investigated the possibility that the Hanle effect could extend in the wings, when a high rate of collisions and strong magnetic fields are present. However they ruled out this explanation when considering realistic collisional rates and field strengths. We finally observe that at the spatial and temporal resolutions of the observations of Bianda et al. (2003) it can be excluded that the detected U/I signals could be produced by horizontal inhomogeneities in the solar plasma.

Theoretical investigations carried out during the last few years (see del Pino Alemán et al. 2016; Alsina Ballester et al. 2016) have shown that, in contrast to what was previously thought, the conspicuous scattering polarization signals observed in the wings of many strong resonance lines should be sensitive to the presence of magnetic fields. This sensitivity arises when longitudinal magnetic fields are present due to the so-called magneto-optical (MO) effects. These effects most notably induce a rotation of the plane of linear polarization (often referred to as Faraday rotation, e.g., Pershan 1967), modifying the Q/I wing signal and giving rise to an appreciable wing signal in U/I . MO effects have been theoretically predicted to have an appreciable impact on the scattering polarization wings of a number of strong resonance lines, including the Mg II k & h lines (del Pino Alemán et al. 2016; Alsina Ballester et al. 2016), the

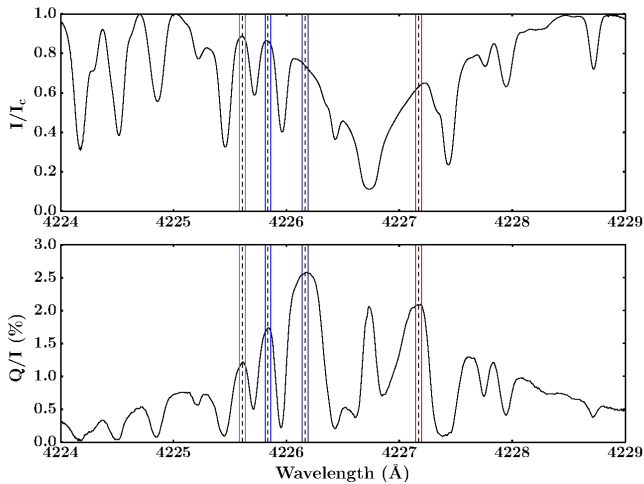


Fig. 1. Intensity spectrum (upper panel) and Second Solar Spectrum (lower panel) across a wavelength interval containing the Ca I 4227 Å line (data from Gandorfer 2002). The blue and red lines indicate the wavelength intervals of interest for this work (see text).

Sr II line at 4078 Å (Alsina Ballester et al. 2017), the H I Ly- α line (Alsina Ballester et al. 2019), and the Ca I line (Alsina Ballester et al. 2018). These theoretical investigations suggest MO effects as an ideal candidate for explaining observations like those of Bianda et al. (2003). Moreover, they could offer a novel window into the magnetism of the solar atmosphere, providing complementary information to that accessible through the Hanle and Zeeman effects.

In this work we present new spectropolarimetric observations of the Ca I 4227 Å line, carried out in regions having different levels of magnetic activity. We provide indications that variations of the Q/I wing lobes, together with the appearance of significant U/I wing signals, are observed in regions where relatively strong longitudinal fields are present, thus supporting the theoretical prediction that such variations are produced by MO effects. In section 2 we analyze the scattering polarization signal of the Ca I 4227 Å line, and we introduce the main physical quantities on which we will base our analysis. In sections 3, 4 and 5 we present our spectropolarimetric observations, which were carried out with the Zurich Imaging Polarimeter (ZIMPOL), both at GREGOR and at IRSOL. For each of them, we briefly describe the instrumental set-up, we provide information on the observed solar region, and we describe the data reduction procedure. Finally, we analyze the data, and we provide our conclusions.

2. The scattering polarization signal of the Ca I 4227 Å line

In the solar intensity spectrum, the Ca I 4227 Å line is characterized by a broad absorption profile with extended wings (see the upper panel of Figure 1). It is produced by a resonance transition between the ground level of neutral calcium, which has total angular momentum $J_\ell = 0$ [1S_0], and an upper level with $J_u = 1$ [1P_1]. The line-core radiation originates primarily from atmospheric heights around 1000 km above the $\tau = 1$ surface, making it chromospheric in nature (Supriya et al. 2014), while the radiation at wavelengths immediately outside the core of the line originates from photospheric heights, as illustrated in Figure 2.

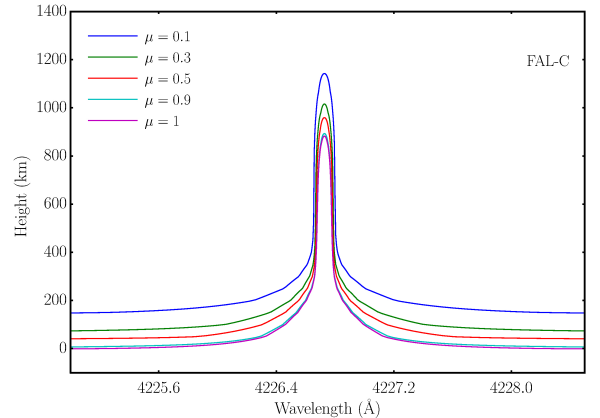


Fig. 2. Height at which the optical depth is unity as a function of wavelength across the Ca I 4227 Å line, in the semi-empirical atmospheric model C of Fontenla et al. (1993), for various lines of sight (see legend). These curves provide a rough estimate of the formation region of the line as a function of wavelength.

This line exhibits the largest scattering polarization signal in the visible range of the so-called Second Solar Spectrum (Brückner 1963; Stenflo et al. 1980, 1984; Gandorfer 2002). The Q/I profile is characterized by a sharp peak in the line core and prominent lobes in the wings (see the lower panel of Figure 1). This characteristic triplet-peak structure is typical of strong resonance lines. The Q/I wing lobes arise as a consequence of frequency coherent scattering processes (Holzreuter et al. 2005). As such, it can be shown that their amplitude is insensitive to the depolarizing effect of elastic collisions with neutral perturbers. On the other hand, elastic collisions may modify the amplitude of the scattering polarization wings through the branching ratios determining the fraction of coherent and non-coherent scattering processes (see Alsina Ballester et al. 2018). The drops in amplitude that can be observed within the wing lobes of the Q/I signal result from the presence of several blended lines, especially of Fe I, which can be clearly observed also in the intensity spectrum.

In this work we search for observational evidences of the theoretically predicted sensitivity of the scattering polarization wing lobes of the Ca I 4227 Å line to MO effects by comparing the spatial variations of the linear polarization signals to the magnetic activity within the same regions. To this aim, we analyze the linear polarization angle (i.e., the angle between the direction of linear polarization and the specified reference direction) and the total linear polarization fraction at particular wing wavelengths. The polarization angle, which is defined within the interval $[0^\circ, 180^\circ)$ (e.g., Landi Degl’Innocenti & Landolfi 2004), is given by

$$\alpha = \frac{1}{2} \tan^{-1} \left(\frac{U}{Q} \right) + \alpha_0, \quad (1)$$

$$\text{with } \alpha_0 = \begin{cases} 0^\circ, & \text{if } Q > 0 \text{ and } U \geq 0 \\ 180^\circ, & \text{if } Q > 0 \text{ and } U < 0 \\ 90^\circ, & \text{if } Q < 0 \end{cases} . \quad (2)$$

According to this definition, when $U/I = 0$, $\alpha = 0^\circ$ if $Q/I > 0$ and $\alpha = 90^\circ$ if $Q/I < 0$, while when $Q/I = 0$, $\alpha = 45^\circ$ if $U/I > 0$, and $\alpha = 135^\circ$ if $U/I < 0$. The linear polarization angle is of course undefined when $Q = U = 0$. The total linear

polarization fraction is given by:

$$P_L = \sqrt{(Q/I)^2 + (U/I)^2}. \quad (3)$$

We note that the total linear polarization fraction of scattering polarization signals depends directly on the degree of anisotropy of the scattered radiation field.

The MO effects operating in the presence of a magnetic field with a longitudinal component produce a rotation of the plane of linear polarization, giving rise to a non-zero α angle. On the other hand, one may in principle expect such MO effects to preserve the polarization fraction P_L . However, it should be noted that the emerging radiation is generally emitted over an extended region in the solar atmosphere. Since the rotation of the plane of linear polarization depends on the distance traveled through the medium, radiation emitted at different points is rotated by different amounts. As a consequence, the total linear polarization fraction of the radiation can decrease (see the Appendix A in Alsina Ballester et al. 2018).

In order to reduce the influence of blends as much as possible, we focus our attention on the wing wavelengths at which the Q/I signal shows local maxima (peaks). We consider four different wavelengths, three in the blue wing (moving from the core to the wing, they will be referred to as bI, bII, and bIII) and one in the red wing (hereafter referred to as rI). Due to the noise affecting the observed profiles, the position of the Q/I peaks is determined by performing a Gaussian fit of the observed signal around the considered peak, and by finding the maximum of the ensuing curve. To minimize the noise in the physical quantities that will be analyzed (α and P_L), the observed signal is averaged over a small spectral interval centered at the fit maximum. The width of this interval must be large enough to reach an acceptable signal-to-noise ratio, but sufficiently narrow to not include spectral regions affected by the blends. We have found a width of 50 mÅ to be suitable. We have verified that the values of α and P_L do not change appreciably if this value is slightly modified. Taking the observation of Gandorfer (2002) as reference, the wing intervals, determined as described above, are shown in Figure 1. Such wing intervals can be specified through their distance from the line center, determined by finding the intensity absorption profile minimum, following a fitting procedure fully analogous to the one previously described. In all the observations considered in this work, the wavelength intervals of interest are determined from the Q/I profiles averaged over the entire slit, following the aforementioned workflow.

3. The Zeeman V/I signal in the nearby Fe I 4224.2 Å line

For the purpose of determining the magnetic origin of the spatial variations of the wing scattering polarization of the Ca I 4227 Å line, we analyze the circular polarization signal produced by the Zeeman effect in the nearby Fe I 4224.2 Å line. Although it must be acknowledged that in general Stokes V is not strictly proportional to the longitudinal component of the magnetic field (see del Toro Iniesta & Ruiz Cobo 2016), it nevertheless provides a reliable indication of the level of magnetic activity of the observed region. For all the measurements presented in the following sections, we have considered the maximum amplitude of the blue peak of the V/I signal of the aforementioned Fe I line, because the red peak is closer to another blended line.

4. Observations at GREGOR

The first observations that we analyze were taken at the GREGOR telescope on June, 24th 2018, using the ZIMPOL camera (see Ramelli et al. 2010), which was installed at the GREGOR spectrograph. The polarimeter analyzer, consisting of a double ferroelectric crystal (FLC) modulator followed by a linear polarizer, was mounted in front of the spectrograph slit after several folding mirrors; the FLC modulates the polarization signals at the frequency of 1 kHz, allowing to “freeze” intensity variations due to seeing (see Ramelli et al. 2014, for technical details).

The spectrograph slit covers a solar area of $\sim 0.3''$ (width of the slit) times $47''$ (length of the slit). The ZIMPOL images presented in this work have 140 pixels along the spatial direction and 1240 pixels along the spectral direction. According to the Nyquist criterion, the attainable spatial resolution is $\sim 0.6''$, while the spectral resolution is of ~ 10 mÅ.

The GREGOR polarimetric calibration unit (GPU, Hofmann et al. 2012) is mounted at the second focal point (F2) before any folding reflection, in order to avoid any significant instrumental polarization produced by the mirrors. Due to the presence of a pre-filter in the GPU that blocks the radiation at all wavelengths below a cutoff just above the Ca I line, the polarimetric calibration measurements were performed at around 4240 Å and not at the exact wavelength of the line. The polarimetric calibration, the dark images and the flat field (obtained by moving the telescope randomly around disc center) were recorded within a few minutes of the observations (see Dhara et al. 2019, for more details).

We carried out two observations: one on an active region close to the West limb, and one on a quiet region at a diametrically opposed position at the East limb. The latter was carried out in order to have an observation in the quiet Sun to be compared to the one in the active region. For scheduling reasons, the observations were carried out around noon, which is a comparatively unfavorable time because the althazimuthal system rotates quite fast. This introduced time-dependent instrumental polarization signals that could not be completely removed in the data reduction. Moreover the seeing was rather poor ($r_0 < 4$), but still good enough for the purpose of this work. The slit was placed parallel to the limb, choosing the positive direction for Stokes Q to be parallel to the slit direction. The tip-tilt of the adaptive optics (AO) system (Berkefeld et al. 2016) was used to keep the limb distance constant with an uncertainty of $\sim 0.5''$. The data of the two observations were corrected using the flat-field and dark image, and a Fourier filter was also used to remove the periodic fringes originated by both electronics and optics. Furthermore, because the absolute value of the polarization cannot be determined with the instrumental set-up used in this campaign, the Stokes profiles of the measurements were properly shifted along the polarization scale so that in the continuum Q/I matches the theoretical value (Gandorfer 2002) while U/I and V/I are zero.

For each Stokes parameter, the statistical error has been determined as follows. A slit portion of 20 pixels, corresponding to a magnetically uniform region, is selected. Then, at each frequency, the standard deviation is taken over the considered portion. The one with the highest occurrence is taken as the statistical error for all frequency points. On the other hand, the statistical error associated to the linear polarization fraction and linear polarization angle is taken as the average absolute difference between such quantities, calculated from the experimental data at the all spatial positions and a smooth function fitting their variation along the slit.

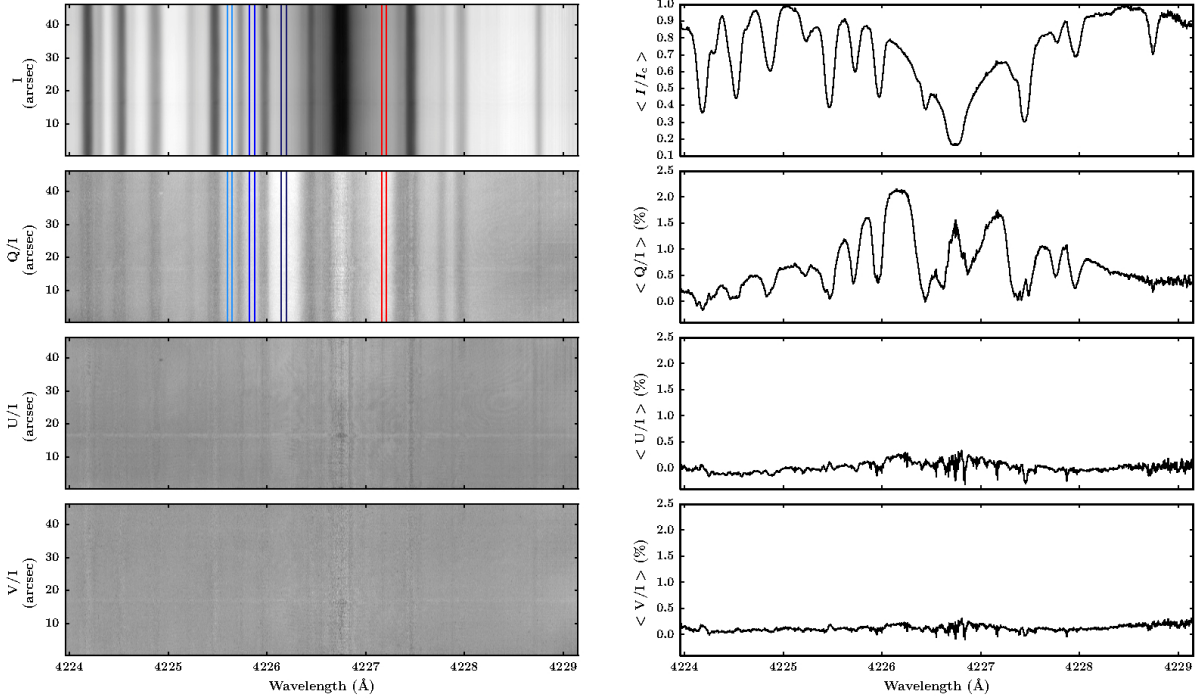


Fig. 3. Stokes I , Q/I , U/I , and V/I images (left) and spatially-averaged profiles (right). The spatial average was performed over the entire slit. The intensity is normalized to the continuum. The observations were taken at $\sim 6''$ from the solar limb, across a quiet region, with the slit oriented parallel to the nearest limb. The positive direction for Stokes Q is taken parallel to the limb. The wavelength intervals of interest are highlighted in the intensity and Q/I images.

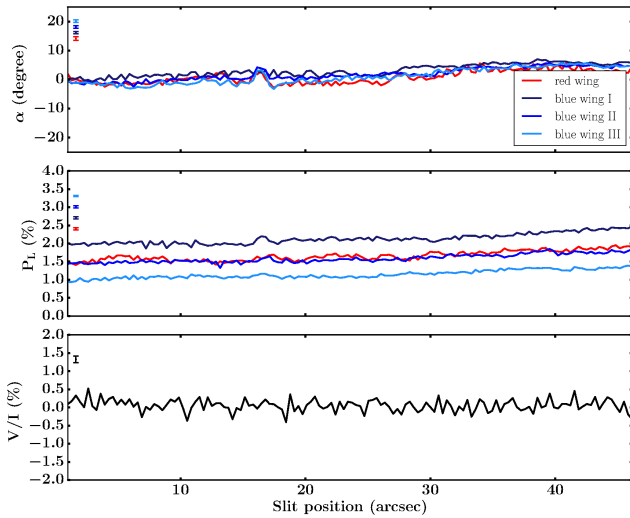


Fig. 4. Linear polarization angle (top panel) and total linear polarization fraction (middle panel) along the slit for the considered wavelength intervals (see text and Table 1). In the bottom panel, the amplitude of the blue peak of the V/I signal in the Fe I 4224.2 Å line is shown as a function of the slit position. The values shown in all three panels are obtained from the data presented in Figure 3. The error bars (statistical error) are reported in the upper left part of each panel.

4.1. GREGOR observation on a quiet region: analysis

We observed a quiet Sun region close to the East limb, at a limb distance of $\sim 6''$. The duration of the measurement was around 8 minutes (240 frames of 1 second exposure time each, with 1 second of lag between two consecutive frames). Figure 3 shows this measurement and the corresponding spatially averaged Stokes profiles. The statistical error was determined as described in section 4. It is 0.09% for Stokes Q/I and V/I and 0.06% for Stokes U/I .

The Stokes Q/I profile shows the aforementioned triple peak structure, with a sharp peak at the line core and extended wing lobes; the highest polarization value in the blue lobe reaches $\sim 2\%$. We notice the persistence of some spurious effects in the U/I and V/I profiles, whose origin can be attributed to the fast changes of the instrumental polarization at the time of day at which the observation was taken (see section 4).

As discussed in section 2, we focus our attention on four wavelength intervals in the wings, which are highlighted in Figure 3 and whose distances from line center are given in Table 1.

Table 1. Wing wavelength intervals for Figure 3.

Wavelength interval	Distance from line center [Å]
bI	0.57
bII	0.89
bIII	1.12
rI	0.44

The upper panel of Figure 4 shows that the linear polarization angle is very close to zero along the whole slit for all the considered wavelengths. The anomalous peak found between 15'' and 17'' is of instrumental origin, resulting from dust grains in the optical system, close to the focal plane. This is supported by the bright horizontal stripe found at the same spatial position in Figure 3. Also the total linear polarization fraction does not show any significant variation along the slit, at any of the considered wavelengths (see middle panel of Figure 4). These results are compatible with our hypothesis because we are observing a quiet Sun region, where no magnetic fields capable of producing significant MO effects are expected. The absence of magnetic fields with a significant longitudinal component is confirmed by the very weak V/I signals observed in the nearby Fe I line (see lower panel of Figure 4).

4.2. GREGOR observation on an active region: analysis

At GREGOR, we also observed a region at 4'' from the West limb with modest magnetic activity, with part of the slit placed upon a region with moderate activity (see slit portion from ~35'' to 47'' in Figure 5). The duration of the measurement was around 9 minutes (284 frames of 1 second exposure time each, with 1 second of lag between two consecutive frames). The statistical error was determined as described in section 4. It is 0.08% for Stokes Q/I and V/I and 0.07% for Stokes U/I .

Figure 5 shows the Stokes images (left panels) and the corresponding spatially averaged profiles (right panels), for which the average was performed within the region where the magnetic field is strongest (i.e., over the slit portion from ~35'' to 47''). In this region, Stokes Q/I shows again a triplet peak structure. However the line core peak, in comparison to the previous measurement (see Figure 3), is clearly depolarized through the Hanle effect, which also induces significant U/I line-core signals. In the line wings prominent U/I signals are found along the entire slit. A significant depolarization of both Q/I and U/I wing signals is found in the region between ~35'' and 47''. Indeed the blue wing maximum of the spatially averaged Q/I signal within this region is significantly smaller than in the previous measurement, being in this case of ~ 0.7%. In the Stokes V/I and Q/I images, the typical patterns of the longitudinal and transverse Zeeman effect, respectively, can be observed.

Table 2. Wing wavelength intervals for Figure 5.

Wavelength interval	Distance from line center [Å]
bI	0.59
bII	0.89
bIII	1.11
rI	0.47

The line-center distance of the wavelength intervals of interest for this observation, as defined in section 2, are shown in Table 2. As can be seen in Figure 6, the polarization angle differs appreciably from zero along the whole slit at all the considered wing wavelengths. This rotation of the plane of linear polarization is compatible with the impact of MO effects produced by a longitudinal magnetic field, whose presence is revealed by the Stokes V/I signal in the photospheric Fe I 4224.2 Å line. An increase of the amplitude of this V/I signal can be clearly observed between ~35'' and 47'', confirming the presence of stronger longitudinal fields in this region (see the bottom panel of Figure 6). It is interesting to observe that while P_L shows a clear decrease

in this region, the variation of the polarization angle is less pronounced. This behavior can be interpreted observing that the anisotropy of the radiation field and other properties of the atmospheric plasma (e.g., the density of neutral perturbers) have a direct impact on P_L , whereas they influence α only through its sensitivity to the magnetic field (Capozzi et al. in preparation). The observed variation of P_L could thus be mainly ascribed to a variation of the properties of the atmospheric plasma in the region between ~35'' and 47'', rather than to the presence of stronger fields via MO effects.

5. Observation at IRSOL

Another set of spectropolarimetric observations of the Ca I line at 4227 Å was performed with the ZIMPOL camera at IRSOL on April 19, 2019. The instrumental set-up was similar to the one used during the GREGOR campaign (section 4), but the polarization modulation was done with a photoelastic modulator (PEM), which modulates the signals with a frequency of 42 kHz, allowing us to minimize spurious effects induced by intensity variations due to the seeing.

The spectrograph slit covered a solar area of 0.5'' (width of the slit) times 180'' (length of the slit). Recalling that the ZIMPOL image has 140 pixels in the spatial direction and 1240 pixels in the spectral direction, the spatial sampling is ~1.47''/pixel, and the spectral resolution is ~10 mÅ. The polarimetric calibration, the dark image and the flat field image (obtained by moving the telescope randomly around disc center) were all recorded within few minutes of the observations. The data was corrected for flat-field and dark images, and a Fourier filter was used. Since the polarimetric calibration unit at IRSOL is mounted after two folding mirrors, some cross-talk is unavoidable. The cross-talk correction was made by performing a rotation around the U and Q axes of the Poincaré sphere until the V/I cross-talk signal was minimized. In the observation that we have analyzed, the cross-talk from V/I to Q/I was corrected by a 6° rotation around the U axis, and the cross-talk from V/I to U/I was corrected by a rotation around the Q axis with an angle of 5.5°.

By using a rotating glass tilt plate based on an elaboration of the slit jaw image, the distance of the limb to the spectrograph slit could be kept constant within an accuracy of ~ 1''. Given the length of the slit of the IRSOL telescope we also corrected for the effects of the curvature of the limb (Bianda et al. 2011).

5.1. Analysis

We observed a region at 5'' from the West limb with moderate magnetic activity. The duration of the measurement was around 7 minutes (200 frames of 1 second exposure time each, with 1 second of lag between two consecutive frames). The slit was placed parallel to the nearest limb, and the reference direction for positive Stokes Q was chosen along the slit. The left panels of Figure 7 show the Stokes images while the right panels show the corresponding profiles spatially averaged over the slit portion between ~110'' and 170'' (i.e. over a region in which we have a strong magnetic field with a fixed polarity). The central peak of this Q/I profile is strongly depolarized through the Hanle effect. The maximum value of Q/I in the blue wing reaches ~1% and prominent U/I signals are also found. In the region from ~ 50'' to ~170'', one can recognize the typical patterns of the longitudinal Zeeman effect in the Stokes V/I image, as well as transverse Zeeman signals in Stokes Q/I and U/I . The statistical error was

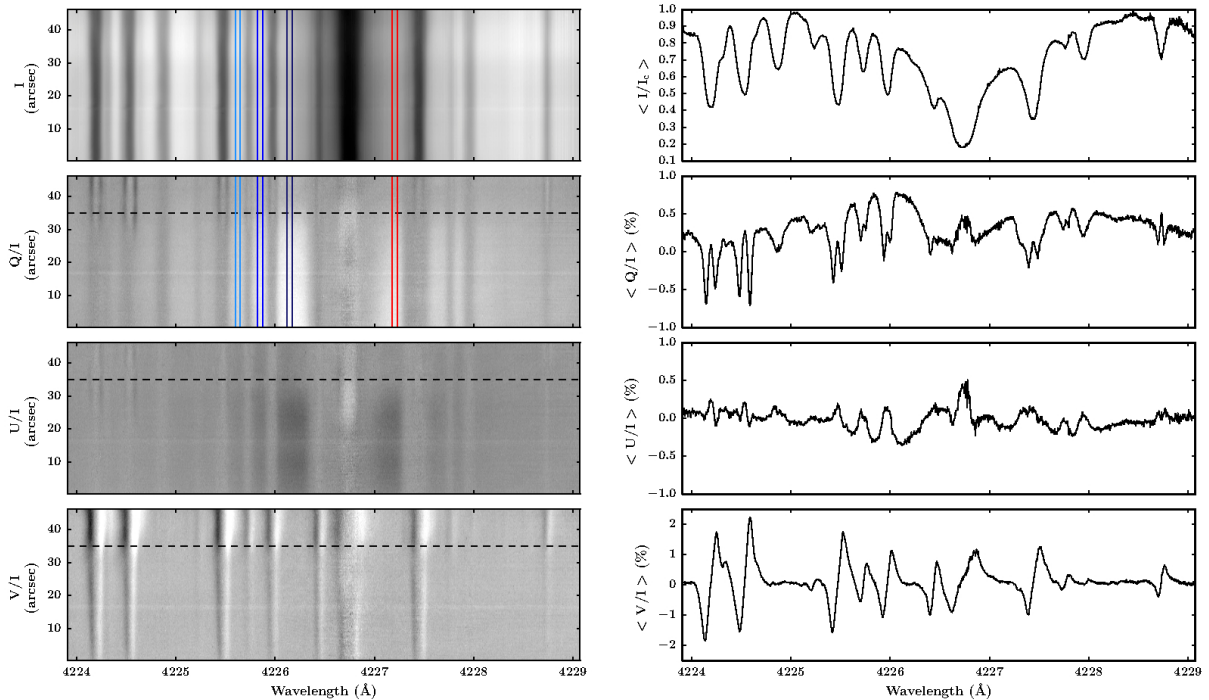


Fig. 5. Stokes I , Q/I , U/I , and V/I images (left) and spatially-averaged profiles (right). The spatial average was performed over the slit positions from $\sim 35''$ to $47''$ (dashed line) where the magnetic field is strongest. The intensity is normalized to the continuum. The observations were taken at a limb distance of $4''$, across a solar region with moderate magnetic activity, with the slit oriented parallel to the nearest limb. The positive direction for Stokes Q is taken parallel to the limb. The wavelength intervals of interest are highlighted in the intensity and Q/I images.

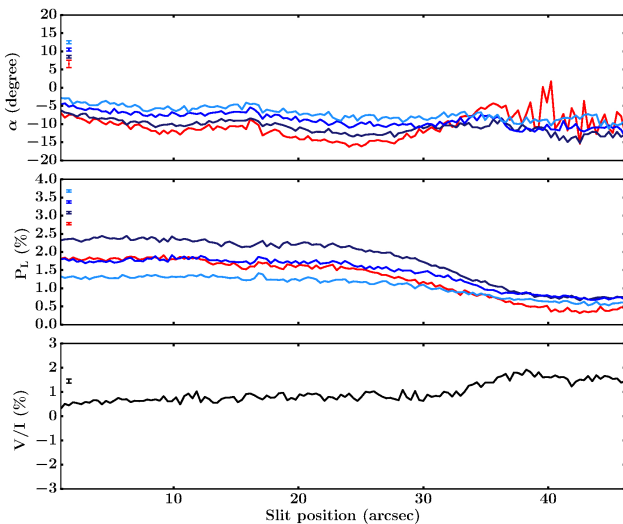


Fig. 6. Linear polarization angle (top panel) and total linear polarization fraction (middle panel) along the slit for the considered wavelength intervals (see text and Table 2). In the bottom panel, the amplitude of the blue peak of the V/I signal in the Fe I 4224.2 Å line is shown as a function of the slit position. The values shown in all three panels are obtained from the data presented in Figure 5. The error bars (statistical error) are reported in the upper left part of each panel.

determined as described in section 4. It is 0.09% for Stokes Q/I and 0.11% for Stokes U/I and V/I .

In Figure 8 the behavior of α , P_L and V/I along the slit is shown. The line-center distance of the wavelength intervals of interest considered in this observation, as defined in section 2, are shown in Table 3.

Table 3. Wing wavelength intervals for Figure 7.

Wavelength interval	Distance from line center [Å]
bI	0.58
bII	0.90
bIII	1.11
rI	0.46

Similarly to what is reported in Sect. 4.2, a clear change in the behavior of both P_L and α can be noticed when going into the more magnetized region, between $\sim 70''$ and $\sim 170''$. The behavior of α closely follows the variations of the V/I signal, including the change of sign in the region around $100''$, strongly suggesting the impact of MO effects. On the other hand, P_L is found to decrease sharply in this region, but it presents no clear variations within it. This could again be an indication that the total linear polarization fraction is mainly determined by the anisotropy of the radiation field and other non-magnetic properties of the plasma (such as the rate of elastic collisions), which we may expect not to vary significantly within the magnetized region. Still focusing on the region around $100''$, we may also propose an alternative explanation (compatible with the previous one). Within this region, one could expect the presence of magnetic fields of opposite polarities below the spatial resolution of the observation, leading to cancellations in both α and V/I (in agreement

with their vanishing values found around $100''$). It is an interesting consequence of MO effects that, if magnetic fields are present such that their orientation changes at scales below the resolution element but above the mean free path of the line's photons, they would still contribute to depolarizing P_L while at the same time cancellations would occur in α (see Appendix A in Alsina Ballester et al. 2018). Discriminating between these two scenarios is outside the scope of this work, but these observational results already provide tantalizing hints about the diagnostic potential of the MO effects.

6. Discussion and conclusions

In the present paper we have analyzed different spectropolarimetric observations of the Ca I 4227 Å line, obtained using the ZIMPOL camera with both the GREGOR and IRSOL telescopes. Spatial variations of the Q/I scattering polarization wing signals as well as the appearance of U/I wing signals, presenting similar spatial fluctuations, have been clearly detected. Comparison with the V/I signals produced by the Zeeman effect in the nearby Fe I 4224.2 Å line clearly indicate that such spatial variations are of magnetic origin, thus supporting the conclusion that they represent measurable signatures of MO effects operating on this line, as theoretically predicted in Alsina Ballester et al. (2018).

To make further advances in this line of investigation it will be of interest to have more quantitative information of the magnetic field present in the observed region. In this regard the use of advanced spatially coherent inversion techniques (e.g. Asensio Ramos & de la Cruz Rodríguez 2015) will be highly beneficial in acquiring much needed information.

The results presented in this work also provide some hints on the potential of MO effects as a novel tool for magnetic field diagnostics, complementary to the Zeeman and Hanle effects. This motivates investigating the impact of MO effects on this line in greater depth. In a forthcoming publication, we will take a numerical approach, based on the solution of the non-LTE radiative transfer problem, in order to characterize the sensitivity of the four Stokes profiles of this line to magnetic fields, accounting for the joint action of the Hanle, Zeeman, and MO effects.

Acknowledgements. This research work was financed by the Swiss National Science Foundation (SNF) through grants 200020_169418 and 200020_184952. E.A.B. and L.B. gratefully acknowledge financial support by SNF through grants 200021_175997 and CRSII5_180238. IRSOL is supported by the Swiss Confederation (SEFRI), Canton Ticino, the city of Locarno and the local municipalities. The 1.5-meter GREGOR solar telescope was built by a German consortium under the leadership of the Kiepenheuer-Institut für Sonnenphysik in Freiburg with the Leibniz-Institut für Astrophysik Potsdam, the Institut für Astrophysik Göttingen, and the Max-Planck-Institut für Sonnensystemforschung in Göttingen as partners, and with contributions by the Instituto de Astrofísica de Canarias and the Astronomical Institute of the Academy of Sciences of the Czech Republic.

References

Alsina Ballester, E., Belluzzi, L., & Trujillo Bueno, J. 2016, ApJ, 831, L15
 Alsina Ballester, E., Belluzzi, L., & Trujillo Bueno, J. 2017, ApJ, 836, 6
 Alsina Ballester, E., Belluzzi, L., & Trujillo Bueno, J. 2018, ApJ, 854, 150
 Alsina Ballester, E., Belluzzi, L., & Trujillo Bueno, J. 2019, ApJ, 880, 85
 Asensio Ramos, A. & de la Cruz Rodríguez, J. 2015, A&A, 577, A140
 Berkefeld, T., Schmidt, D., Soltau, D., Heidecke, F., & Fischer, A. 2016, in Society of Photo-Optical Instrumentation Engineers (SPIE) Conference Series, Vol. 9909, Proc. SPIE, 990924
 Bianda, M., Ramelli, R., Stenflo, J. O., et al. 2011, in ASP Conf. Ser., Vol. 437, Solar Polarization 6, ed. J. R. Kuhn, D. M. Harrington, H. Lin, S. V. Berdyugina, J. Trujillo Bueno, S. L. Keil, & T. Rimmele, 67

Bianda, M., Stenflo, J. O., Gandorfer, A., & Gisler, D. 2003, in ASP Conf. Ser., Vol. 286, Current Theoretical Models and Future High Resolution Solar Observations: Preparing for ATST, ed. A. A. Pevtsov & H. Uitenbroek, 61
 Brückner, G. 1963, ZAp, 58, 73
 del Toro Alemán, T., Casini, R., & Manso Sainz, R. 2016, ApJ, 830, L24
 del Toro Iniesta, J. C. & Ruiz Cobo, B. 2016, Living Reviews in Solar Physics, 13, 4
 Dhara, S. K., Capozzi, E., Gisler, D., et al. 2019, A&A, 630, A67
 Fontenla, J. M., Avrett, E. H., & Loeser, R. 1993, ApJ, 406, 319
 Gandorfer, A. 2002, The Second Solar Spectrum: A high spectral resolution polarimetric survey of scattering polarization at the solar limb in graphical representation. Volume II: 3910 Å to 4630 Å (vdf ETH)
 Hofmann, A., Arlt, K., Balthasar, H., et al. 2012, AN, 333, 854
 Holzreuter, R., Fluri, D. M., & Stenflo, J. O. 2005, A&A, 434, 713
 Landi Degl'Innocenti, E. & Landolfi, M. 2004, Polarization in Spectral Lines (Dordrecht: Kluwer)
 Pershan, P. S. 1967, Journal of Applied Physics, 38, 1482
 Ramelli, R., Balemi, S., Bianda, M., et al. 2010, in Proc. SPIE, Vol. 7735, Ground-based and Airborne Instrumentation for Astronomy III, 77351Y
 Ramelli, R., Gisler, D., Bianda, M., et al. 2014, in Society of Photo-Optical Instrumentation Engineers (SPIE) Conference Series, Vol. 9147, Proc. SPIE, 91473G
 Sampoorana, M., Stenflo, J. O., Nagendra, K. N., et al. 2009, ApJ, 699, 1650
 Stenflo, J. O. 1982, Sol. Phys., 80, 209
 Stenflo, J. O., Baur, T. G., & Elmore, D. F. 1980, A&A, 84, 60
 Stenflo, J. O., Solanki, S., Harvey, J. W., & Brault, J. W. 1984, A&A, 131, 333
 Supriya, H. D., Smitha, H. N., Nagendra, K. N., et al. 2014, ApJ, 793, 42
 Trujillo Bueno, J. 2001, in ASP Conf. Ser., Vol. 236, Advanced Solar Polarimetry – Theory, Observation, and Instrumentation, ed. M. Sigwarth, 161

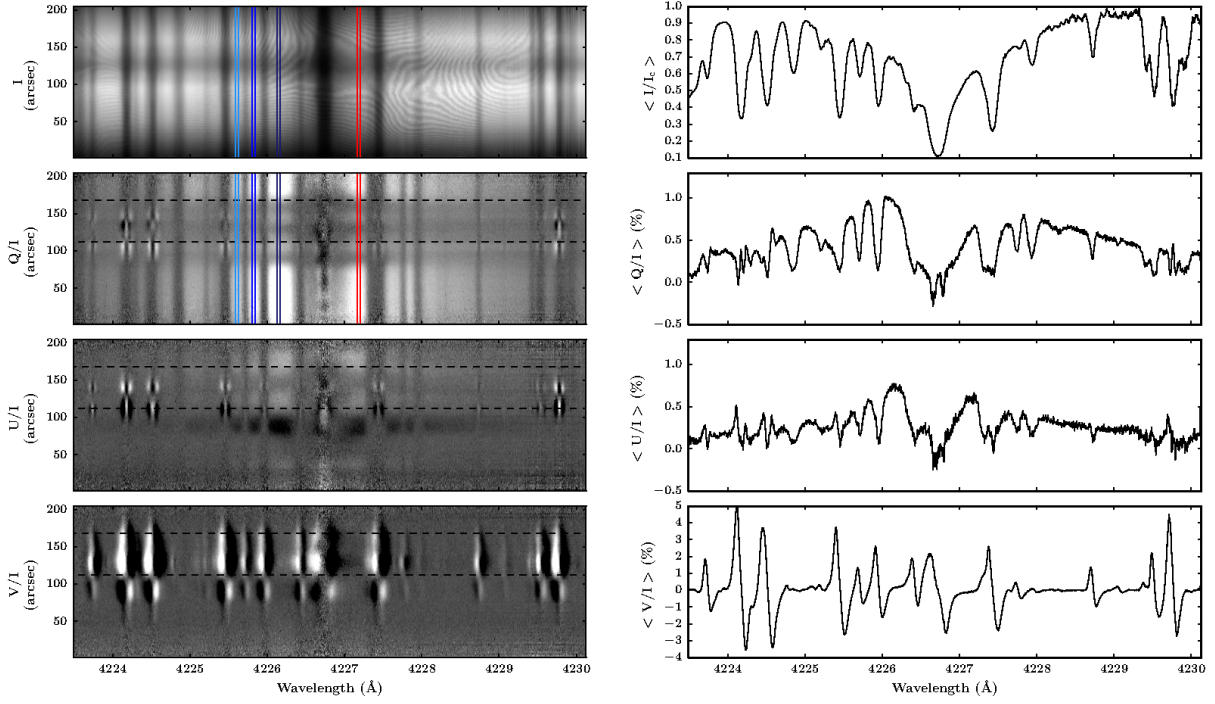


Fig. 7. Stokes I , Q/I , U/I , and V/I images (left) and spatially-averaged profiles (right). The spatial average was performed over the slit positions from $\sim 110''$ to $170''$ (dashed line) where the magnetic field is strongest. The intensity is normalized to the continuum. The observation was taken at a limb distance of $5''$, across a solar region with stronger magnetic activity, with the slit oriented parallel to the nearest limb. The positive direction for Stokes Q is taken parallel to the limb. The wavelength intervals of interest are highlighted in the intensity and Q/I images.

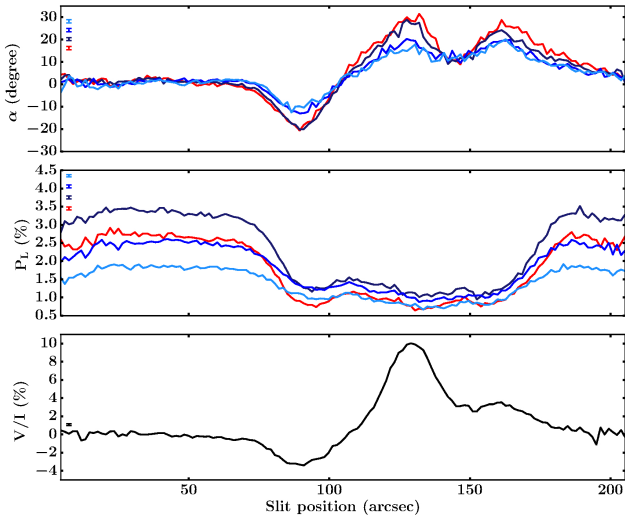


Fig. 8. Linear polarization angle (top panel) and total linear polarization fraction (middle panel) along the slit for the considered wavelength intervals (see text and Table 3). In the bottom panel, the amplitude of the blue peak of the V/I signal in the Fe I 4224.2 Å line is shown as a function of the slit position. These values are obtained from the data presented in Figure 7. The error bars (statistical error) are reported in the upper left part of each panel.